# Time-resolved specular and off-specular neutron reflectivity measurements on deuterated polystyrene and poly(vinyl methyl ether) blend thin films during dewetting process

Hiroki Ogawa,[1] Toshiji Kanaya,[1,a)] Koji Nishida,[1] Go Matsuba,[1] Jaroslaw P. Majewski,[2] and Erik Watkins[2]
[1]*Institute for Chemical Research, Kyoto University, Uji, Kyoto-fu 611-0011, Japan*
[2]*LANSCE, Los Alamos National Laboratories, Los Alamos, New Mexico 87545, USA*

(Received 26 June 2009; accepted 18 August 2009; published online 14 September 2009)

We performed time-resolved specular and off-specular neutron reflectivity measurements on blend thin films 42 and 98 nm thick of deuterated polystyrene and poly(vinyl methyl ether) during dewetting process induced by the phase separation in two phase region using a time-of-flight neutron reflectometer. In the specular measurements we found that the phase separation directed to the depth direction occurred near the air interface as well as near the Si substrate during the incubation period before dewetting. In addition we also found that the phase separation occurred asymmetrically at the two interfaces and inhomogeneously in the film plane, showing that the dewetting was induced by the composition fluctuation mechanism. Off-specular reflectivity was analyzed, for the first time, to evaluate kinetics of structure formation in the film plane during the dewetting process. We found in the analysis that the droplets formation in micrometer scale occurred in the late stage of dewetting. © *2009 American Institute of Physics*. [doi:10.1063/1.3224125]

## I. INTRODUCTION

Polymer thin films consisting of single component and multicomponents are of great interest[1–4] because properties of polymer thin films are very different from bulk, and directly related to many important phenomena such as coating, adhesive, surface friction, lubricants, and dielectric layer. Studies on polystyrene (PS) thin films supported on Si substrates have revealed that the glass transition temperature $T_g$ decreased with film thickness below about 40 nm.[5–9] Much larger decrease in $T_g$ was reported for free standing PS films by Forrest and co-workers.[7,10,11] However, the glass transition temperature increased with decreasing film thickness for poly(methyl methacrylate) (PMMA)[5,6] showing the importance of interactions between polymer and substrate. Recently, dewetting and phase separation of polymer blend thin films are also of great interest from viewpoints of industrial applications as well as fundamental investigations. The dewetting of the phase separated polymer blend thin film limits the industrial applications because they require stable, homogeneous, and uniform thin films. This motivated the fundamental studies of polymer blend thin films very much to reveal the dewetting mechanism and control the morphology[4] for blend thin films of poly(*p*-methylstyrene) (PpMS) and deuterated PS (dPS),[12] poly (styrene-ran-acrylonitrile) and deuterated poly (methyl methacrylate),[13–17] and PS and poly (vinyl methyl ether) (PVME)[18–23] in various film thickness ranges.

In a previous paper,[22] we investigated morphology and kinetics of phase separation as well as dewetting in blend thin films of PS/PVME in two phase region in a wide film thickness $d$ range from 65 $\mu$m to 42 nm ($\sim 2.5R_g$; $R_g$ being radius of gyration of a polymer chain) to elucidate the relation between phase separation and dewetting. We found that the dewetting occurred after a long incubation time in a thickness range below $\sim$200 nm, suggesting some structure formation occurred in the depth direction during the incubation period before the dewetting. In order to see what structure formation occurs in the incubation period we performed neutron reflectivity measurements on blend thin films of dPS and PVME.[23] The measurements were done by quenching the samples after annealing in two phase region for a give period. We found that the phase separation in the depth direction occurred during the incubation period before dewetting. This result suggests that the dewetting in the dPS/PVME blend thin films occurs in the composition fluctuation mechanism[24–28] rather than the capillary wave fluctuation mechanism.[15,16]

In this work, we performed time-resolved specular and off-specular neutron reflectivity measurements on the dewetting process of dPS/PVME blend thin films 42 and 98 nm thick in two phase region using a time-of-flight (or energy dispersive) neutron reflectometer to study the details of phase separation in the depth direction before dewetting observed in the previous measurements.[23] In addition, we analyzed, for the first time, the off-specular data to demonstrate that the time-of-flight reflectivity measurements are very powerful to investigate kinetics of structure formation in the film plane in micrometer scale.

a)Electronic mail: kanaya@scl.kyoto-u.ac.jp.

 

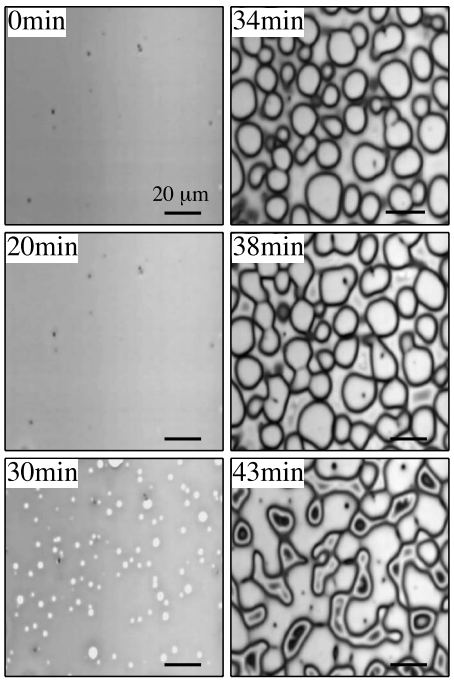


FIG. 1. Time evolution of CLSM images for 98 nm blend thin film of dPS and PVME at 125 °C.

## II. EXPERIMENTAL

dPS and PVME used in this study have weight-average molecular weights $M_w$=280 000 and 90 000, and the molecular weight distributions $M_w/M_n$=1.08 and 1.88, respectively, where $M_n$ is number-average molecular weight. Both dPS and PVME were purchased from Scientific Polymer Products, Inc. and were purified by precipitating the toluene solutions into excess methanol and *n*-heptane several times, respectively, and dried in vacuum at room temperature for 72 h. It is noted that dPS and PVME used in this experiment have similar values of radius of gyration $R_g$, which are 8.3 and 8.1 nm, respectively, although their molecular weights are different. Blend films were prepared by spin-coating the toluene solution of dPS and PVME on a cleaned Si wafer with native oxide layer after filtering with 2 $\mu$m pore size membrane at room temperature. The films were then annealed at 60 °C for 24 h after drying in vacuum at room temperature for 24 h. Thickness of polymer film was controlled by varying the polymer concentration in solution and confirmed with ellipsometer measurements. In the study we prepared blend thin films 42 and 98 nm thick. dPS/PVME bulk blend has a lower critical solution temperature type phase diagram, and the estimated critical weight fraction of dPS $\phi_{\mathrm{dPS}}$ is 0.3 and the critical temperature $T_c$ is 111 °C. All the measurements were done on the blend samples with the critical concentration.

Neutron reflectivity measurements were performed with the surface profile analysis reflectometer (SPEAR) (Ref. 29) at Los Alamos Neutron Science Center (LANSCE), Los Alamos National Laboratories, which is a time-of-flight (TOF) or energy dispersive reflectometer. Time-resolved measurements were started just after temperature jump from room temperature to a given temperature in the two phase region. The duration time for the one measurement was 5–10 min and the $Q_z$ range in the specular reflectivity measurements was from 0.1 to 0.7 $\mathrm{nm}^{-1}$ with glancing angle $\theta_i$ of 0.2° (see Fig. 8).

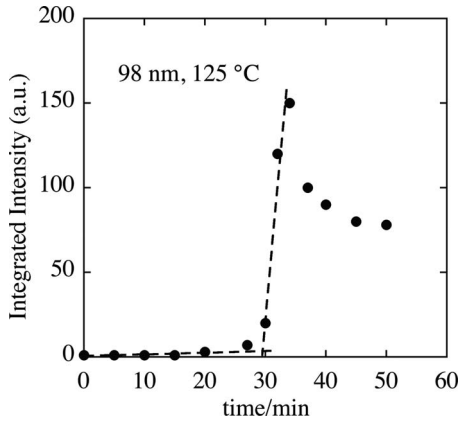


FIG. 2. Integrated intensity of FFT of the CLSM images for 98 nm blend thin film of dPS and PVME as a function of annealing time at 125 °C. The estimated incubation time before dewetting is 29 min.

Confocal laser scanning microscope (CLSM) measurements were done using LASER TECH. ILM15 on the dPS/PVME thin films during the dewetting process. Atomic force microscope (AFM) measurements were performed at room temperature after quenching the sample from two phase region using JEOL JSPM-4200 to examine the surface morphology of the films.

## III. RESULTS AND DISCUSSION

We first performed CLSM measurements on the dPS/PVME thin films to estimate the incubation period before dewetting after temperature jump into two phase region from one phase region. The time evolutions of the CLSM images are shown in Fig. 1 for the 98 nm film after temperature jump to 125 °C. It is evident that nothing happened before 20 min at least in the CLSM image, while at 30 min we clearly observed some holes in the film due to dewetting, which rapidly grew in size with annealing time. In order to estimate the incubation time before the dewetting we performed fast Fourier transform (FFT) of the CLSM images and the integrated intensity was plotted in Fig. 2 as a function of annealing time. The integrated intensity abruptly begins to increase at a certain annealing time. Extrapolating the intensities in the incubation period and in the dewetting period we define the incubation time as a crossing time of the two lines as shown in Fig. 2. According to the definition the incubation time was 29 min for the 98 nm film at 125 °C. In this paper we use this definition for the incubation time. When the incubation time is defined as an onset time of the integrated intensity, it is ~25 min. Similar experiments were done for the 98 and 42 nm films at 115, 125, and 135 °C. The incubation times thus estimated are 66, 29, and ~6 min for the 98 nm film at 115, 125, and 135 °C, respectively, and 120, 49, and ~11 min for the 42 nm film at 115, 125, and 135 °C, respectively. In any case, the 98 and 42 nm films show very long incubation times before dewetting after temperature jump into the two phase region.

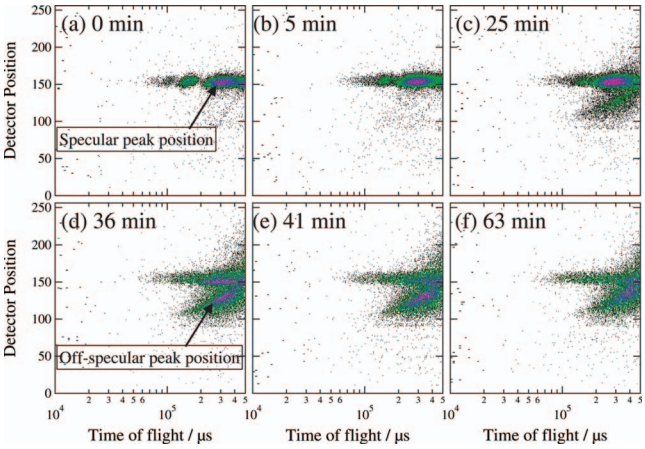


FIG. 3. Time evolution of raw 2D data obtained by SPEAR at LANSCE during dewetting process for 42 nm blend thin film of dPS and PVME at 135 °C in two phase region.

In order to see what happened in the incubation period, we have performed time-resolved neutron reflectivity measurements on the blend thin films after temperature jump into two phase region using a TOF (or energy dispersive) neutron reflectometer SPEAR at LANSCE, Los Alamos National Laboratory. In the measurements reflected neutron intensities were recorded as functions of one-dimensional (1D) detector position and neutron TOF (or neutron wavelength or neutron energy). The raw two-dimensional (2D) data are shown in Fig. 3 for the 42 nm film during the annealing process after the temperature jump to 135 °C. Just after the temperature jump (0 min) we observed oscillatory intensity along the TOF axis at a detector pixel of about 153, which corresponds to the specular reflection. This specular reflectivity profile gives us information about the scattering length density or the composition fluctuations along the depth direction ($z$ direction). As the annealing proceeded, we observed off-specular reflectivity component apart from the specular one [see Fig. 3(d)], and it seems that the off-specular component has a peak in the intensity profile, which is indicated by an arrow in the figure. As will be seen later we will analyze the off-specular data to obtain the structure information in the film plane ($x$-$y$ directions). First we analyze the specular data to discuss the time evolution of composition fluctuations along the depth direction ($z$ direction).

In Fig. 4 we plotted 1D specular reflectivity profiles for the 98 nm film as a function of $Q_z$ at various annealing times after the temperature jump into two phase region (125 °C). Just after the temperature jump (0 min) the well-defined fringed pattern was observed in the profile. As the annealing proceeded, the fringed pattern was gradually smeared even in the incubation period until 29 min, suggesting that the surface and/or interfacial roughness increased before dewetting. At last no fringed patterns were observed in the reflectivity profile at 32 min, showing that the film was completely dewetted. This agrees with the CLSM observation (see Fig. 2). It should be noted that the reflectivity profile at 124 min has a long oscillatory component, suggesting that a very thin layer was again formed on the substrate after the dewetting. This problem will be discussed later.

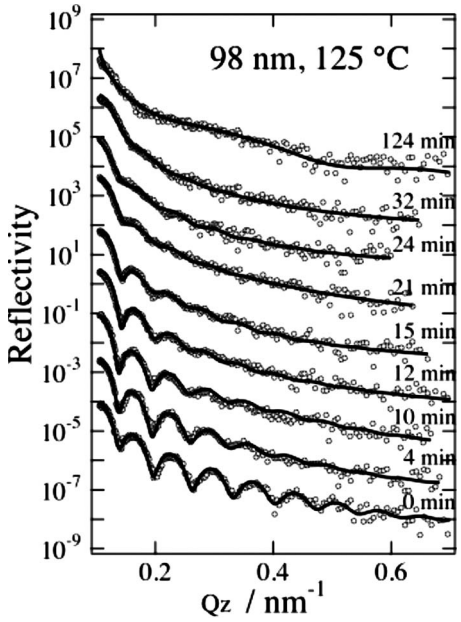


FIG. 4. Time evolution of 1D specular neutron reflectivity profiles during dewetting process for 98 nm blend thin film of dPS and PVME at 125 °C in two phase region. Solid curves are the results of fit with the trilayer model (see text).

As shown in a previous paper[23] the specular reflectivity profile could be described by a trilayer model consisting of surface PVME layer at air, middle blend layer, and interface PVME layer at Si substrate even in the one phase region because preferential interactions are considered between PVME and air[30–34] and between PVME and Si substrate.[19,20] In the trilayer model the surface roughness and the interface roughness were introduced by an error function. In the present analyses, therefore, the trilayer model was employed and fitted to the observed reflectivity profiles, and the results of fits are shown by solid curves in Fig. 4, showing good fitness. The depth profiles of the scattering length densities evaluated in the fits are shown in Fig. 5 at various annealing times for the 98 nm film at 125 °C. The estimated surface and interface PVME layers at 0 min are ~4 and ~5 nm thick, agreeing with the previous measurements using a re-

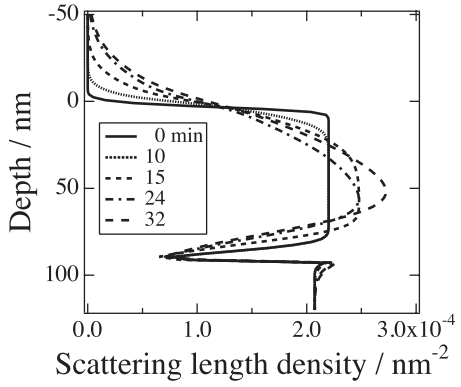


FIG. 5. Time evolution of depth profile of scattering length density during dewetting process for 98 nm blend thin film of dPS and PVME at 125 °C in two phase region. These were evaluated from fits of trilayer model to the observed reflectivity profiles in Fig. 4.

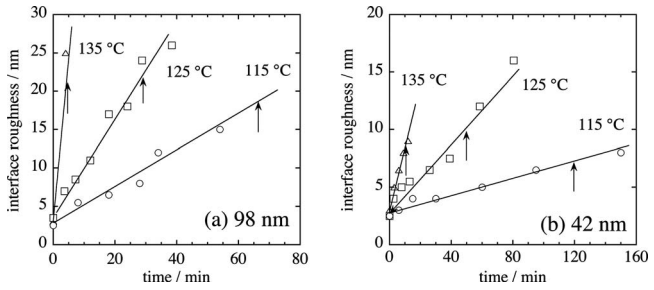


FIG. 6. Time evolution of top interface roughness (interface roughness between the top PVME layer and the middle blend layer) at 115, 125, and 135 °C. (a) 98 nm and (b) 42 nm blend thin films of dPS and PVME.

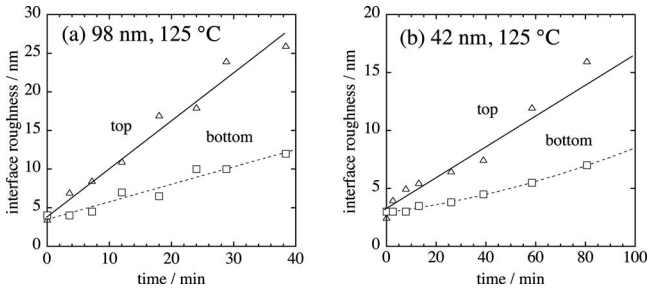


FIG. 7. Time evolution of top interface roughness (interface roughness between the top PVME layer and the middle blend layer) and the bottom interface roughness (interface roughness between the middle blend layer and the bottom PVME layer) at 125 °C. (a) 98 nm and (b) 42 nm blend thin films of dPS and PVME.

flectometer MINE at JRR3 reactor.[23] As the annealing proceeds the interface roughness between the top PVME layer and the middle blend layer (*top interface* roughness) and that between the middle blend layer and the bottom PVME layer (*bottom interface* roughness) increases, showing the phase separation proceeds in the depth direction before dewetting. To see the phase separation in the depth direction more quantitatively, the time evolution of the *top interface* roughness is shown in Figs. 6(a) and 6(b) for the 98 nm film and the 42 nm film, respectively, at 115, 125, and 135 °C. The induction times are shown in the figures by up arrows, which were estimated from the CLSM measurements as mentioned above. The values of the roughness when the dewetting begins are roughly ~20 and ~8 nm for the 98 and 42 nm films, respectively. The increase in the interface roughness is clearly observed even at the early stage in the incubation period for both the 98 and 42 nm films, suggesting that the phase separation of the middle blend layer proceeds along the depth direction even in the incubation period before dewetting. It should be noted that this phase separation does not occur coherently within the film plane. If phase separation directed to the depth direction occur coherently in the film plane we must have observed new oscillatory period corresponding to the characteristic length of the phase separation. This type of phase separation, the so-called surface-directed spinodal decomposition type phase separation, was reported for rather thick blend films.[35] However, this is not the case, and the present observation implies that the phase separation directed to the depth direction in the dPS/PVME thin film dose occurs incoherently in the film plane. The incoherent phase separation in the film plane may support the composition fluctuation dewetting mechanism.[24–27] In this mechanism polymers with preferable interactions with the surface (or the substrate) diffuse to the surface (or the substrate) so as to create the composition gradient across the film. The diffusion could not occur homogeneously over the film surface to create the composition fluctuations in the mixture along the surface. When the amplitude of the fluctuations is large enough, the free surface is eventually destabilized, leading to the dewetting.[24–27] Such mechanism is expected in the dPS/PVME thin film because of the inhomogeneous phase separation in the film plane.

The time evolution of the bottom interface roughness is different from that of the top interface roughness. In order to show the difference, the time evolutions of the top and bottom interface roughnesses are compared in Figs. 7(a) and 7(b) for the 98 and 42 nm films at 125 °C, respectively. The top interface roughness begins to increase with the annealing time just after the temperature jump while the bottom interface roughness stays almost constant in the beginning of the annealing and slowly increases. This result shows that the phase separation near the substrate is obstructed compared with that near the air surface, resulting in asymmetric depth profiles of the scattering length. This is clearly seen in the time evolution of the depth profiles of scattering length density in Fig. 5. This asymmetry of composition fluctuations must be caused by the difference of molecular mobility between near the air surface and near the Si substrate. It is considered that the molecular mobility near the substrate is lower than that near the surface because the degrees of freedom for molecular mobility are less near the hard wall than the air surface (hard wall effect). Hence, the growth of composition fluctuations near the Si substrate is delayed due to the lower mobility. In fact, lower molecular mobility near solid substrate has been often reported for polymer thin films.[36–39]

Comparing the time evolutions of the interface roughness between the 98 and 42 nm films, the roughness in the 98 nm film increases more rapidly in both the top and bottom interfaces than the 42 nm film. The surface and interface PVME layers are almost identical in thickness for the 98 and 42 nm films. Therefore, the difference must be due to the middle blend layer. The dPS or PVME fraction in the middle blend layer, of course, is affected by existence of the top PVME layer at the air and the bottom PVME layer at the Si substrate, especially for very thin films. We have calculated the dPS fraction in the middle blend layer based on the thickness of top and bottom PVME layers to be 0.31 and 0.37 for the 98 and 42 nm, respectively. If we assume the critical concentration of dPS is the same as that in bulk (=0.30), the fraction of 0.37 in the 42 nm film is far from the critical concentration, and hence the quenching depth from the binodal line is smaller in the 42 nm film than in the 98 nm film. This must lead to the slower growth of phase separation in the 42 nm film.

As mentioned above and shown in a previous paper[23] the fringed pattern with a long period was observed in the very late stage after dewetting. In this measurement we also observed the fringed pattern with a long period in both the 98 and 42 nm (see the profile at 124 min in Fig. 4). The fringed

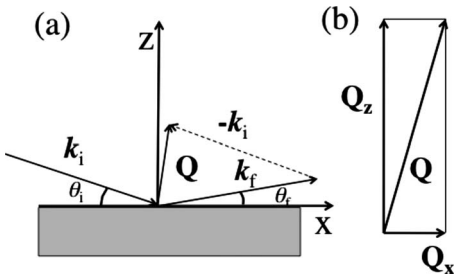


FIG. 8. (a) Reflectivity configuration for off-specular position. (b) $\boldsymbol{Q}_x$ and $\boldsymbol{Q}_z$ components in scattering vector $\boldsymbol{Q}$.

pattern with a long period suggests that a very thin PVME layer was formed in the very late stage. The thickness evaluated by fitting is ~13 nm. Why such a thin layer is formed after the dewetting? In the incubation period the phase separation occurs mainly in the depth direction, but when the dewetting occurs after the incubation the phase separation is not completed. After the dewetting into the droplets the phase separation may proceed within the droplets. Outer surface of the droplets must be PVME because of the preferential interactions between PVME and air.[30–34] The phase separation further proceeds and the surface PVME increases in thickness. Finally PVME comes out from the surface of the droplets onto the substrate to form a very thin layer ~10 nm thick. Similar thin film formation was reported by Stamm and co-workers[12] after a very long annealing of PpMS and dPS blend thin film.

Next, we analyze the off-specular reflectivity to discuss the structure development in the film plane. In order to explain our analysis scattering geometry for the off-specular reflection is described in Fig. 8. In specular configuration, scattering vector $\boldsymbol{Q}$ dose include only $\boldsymbol{Q}_z$ component, but not $\boldsymbol{Q}_x$ one because $\theta_i = \theta_f$, where $\theta_i$ and $\theta_f$ are the glancing angle and 90°-reflection angel, respectively. On the other hand, in off-specular configuration, scattering vector $\boldsymbol{Q}$ includes small $\boldsymbol{Q}_x$ component as shown in Fig. 8(b). The lengths of $\boldsymbol{Q}_x$ and $\boldsymbol{Q}_z$ can be easily calculated using the following relations:

$$\boldsymbol{Q} = \boldsymbol{k}_f - \boldsymbol{k}_i, \tag{1}$$

$$Q_x = \frac{2\pi}{\lambda}(\cos\,\theta_f - \cos\,\theta_i), \tag{2}$$

$$Q_z = \frac{2\pi}{\lambda}(\sin\,\theta_f - \sin\,\theta_i). \tag{3}$$

Using these relations we have translated the raw 2D data (detector position and neutron TOF data) into $Q_z$-$Q_x$ data. The $Q_z$-$Q_x$ plots of the reflective intensities are shown in Fig. 9 for the 40 nm film annealed at 135 °C. It is noteworthy to point out that $Q_x$ value in the measurements is very small in the range of 0.0001 to 0.001 $nm^{-1}$, corresponding to micrometer scale in real space. Therefore, analyzing the off-specular intensity in the $Q_x$ direction we obtain information on the structure development in micrometer scale in the film plane. The present measurement is a kind of out-of-plane grazing incidence small-angle neutron scattering measurements. We plotted the off-specular intensity $I(Q_x)$ against $Q_x$ in Figs. 10(a) and 10(b) for the 98 nm film and 42 nm film at 125 °C, respectively, after integrating the data in a $Q_z$ range of 0.1 to 0.14 $nm^{-1}$. In the beginning of annealing the off-specular intensity is very weak although the intensity near $Q_x$=0 is strong due to the tail of specular reflection. With passing the annealing time by the off-specular intensity gradually increases and a broad peak appears in the profile and shifts to lower $Q_x$ with the annealing time.

In order to see the characteristic features of the off-specular scattering profile $I(Q_x)$ the integrated intensity at around the peak ($Q_x$=0.0001–0.0006 $nm^{-1}$) and the peak position are plotted against the annealing time in Figs. 11(a) and 11(b), respectively. The data points are rather scattered

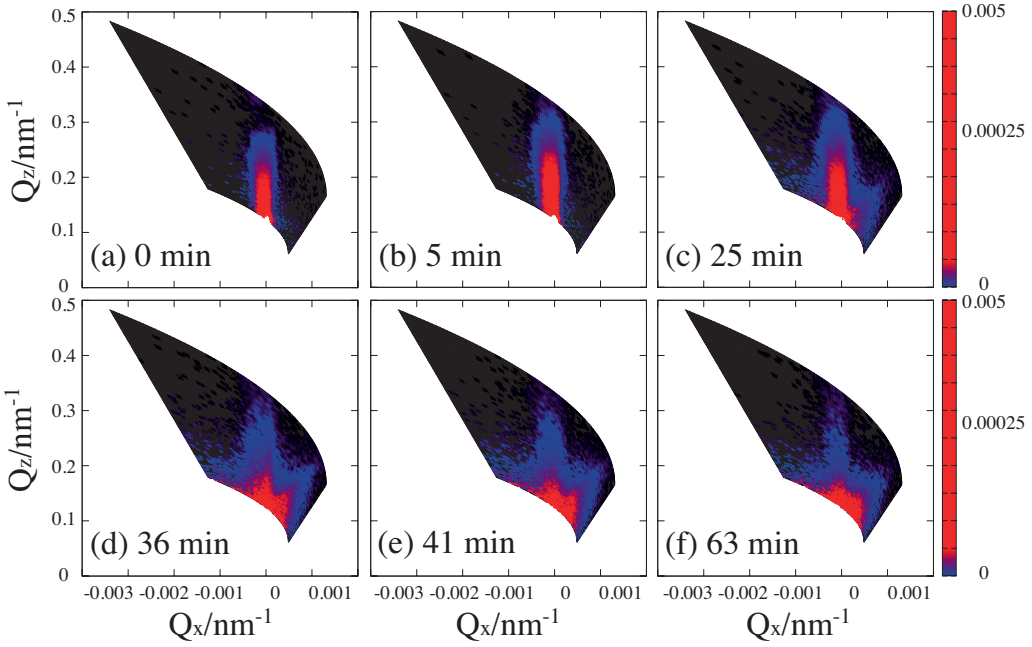


FIG. 9. Time evolution of 2D reflectivity intensity in $Q_x$-$Q_z$ space for 42 nm blend thin film of dPS and PVME at 135 °C.

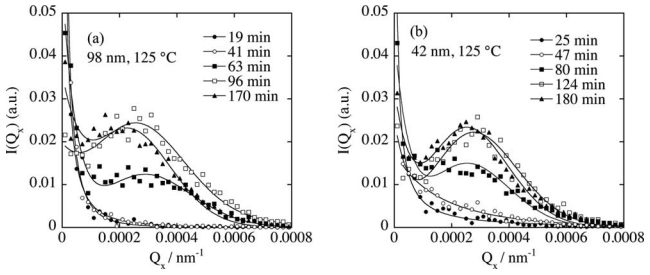


FIG. 10. Time evolution of off-specular intensity $I(Q_x)$ at 125 °C. (a) 98 nm and (b) 42 nm blend thin films of dPS and PVME. Solid curves are drawn by eye.

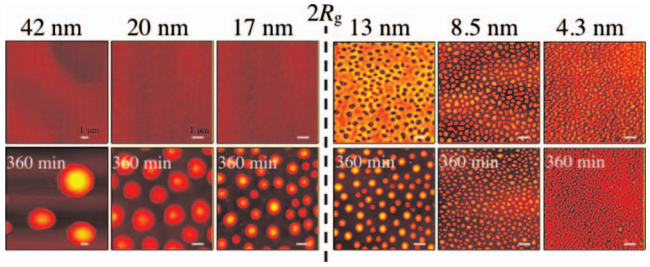


FIG. 12. AFM images of blend thin films of dPS and PVME before and after annealing at 115 °C for 360 min for various initial film thicknesses above and below twice $R_g$ (=17 nm). Scale bars in images are 1 $\mu$m.

due to the weak off-specular intensity, and hence the following discussions are rather qualitative. After the temperature jump to a given temperature in two phase region, the off-specular intensity is almost constant during the incubation period; for example, the incubation time of the 98 nm film at 125 °C is 29 min [see Fig. 11(a)]. However, the intensity gradually increases with annealing time after the incubation period and begins to increase abruptly at a certain annealing time after the incubation period. According to the abrupt increase in the off-specular intensity a broad peak appears in the profile, implying that some ordered structure is formed in the film plane. The peak position gradually shifts to lower $Q_x$ with increasing the annealing time as seen in Fig. 11(b), suggesting the increase in structure in size, and levels off to a certain value. For example, the final peak position is $\sim$0.000 19 nm$^{-1}$ for the 90 nm film at 125 °C, corresponding to $\sim$33 $\mu$m in real space.

In order to reveal what structure was observed in the off-specular intensity we performed AFM measurements on the dPS/PVME blend thin films before and after annealing under the same annealing condition as the reflectivity measurements. In Fig. 12 the observed AFM images are shown for blend films with various film thicknesses before and after annealing at 115 °C for 360 min. It is interesting that thick films above 17 nm have homogeneous flat surfaces before annealing, but thin films below $\sim$13 nm show dewetted surface even just after spin-coating before annealing. It is worth pointing out that 17 nm just corresponds to twice radius of gyration $2R_g$ of dPS and PVME chains. This thickness dependence of the initial surface structure is very interesting but is out of scope of this paper. We will report the results elsewhere. After annealing at 115 °C for 360 min droplets are formed due to the dewetting in both the thin and thick films. The droplets are located rather regularly while the size and the interdroplet distance depend on the initial film thickness very much. Performing FFT of the AFM images of the annealed films, we calculated the expected scattering profiles in the $Q_x$ direction and found that they had a broad peak in the intensity profile corresponding to the droplet-droplet correlation. The evaluated peak position $Q_m$ is plotted in Fig. 13 as a function of the initial film thickness. The position $Q_m$ is roughly proportional to the second power of the film thickness as shown by a straight line in Fig. 13. Here we also plotted the peak position observed in the off-specular intensity profile for the 42 nm film at 115 and 125 °C and for the 98 nm film at 125 °C. The peak positions in the off-specular intensity profile are almost identical to those evaluated from the AFM measurements, concluding that we observed the droplet-droplet correlation in the off-specular reflectivity measurements. The CLSM images (Fig. 1) showed that holes were formed on the film surface in the beginning of dewetting and gradually change to droplets (Fig. 13). As mentioned above the off-specular reflectivity intensity has no peak and the intensity is rather weak in the beginning of dewetting. This must be due to the weak scattering contrast of holes and irregular holes formation in the film plane. In conclusion, in the present off-specular reflectivity measurements, we mainly observed the droplet formation in the late stage of the dewetting.

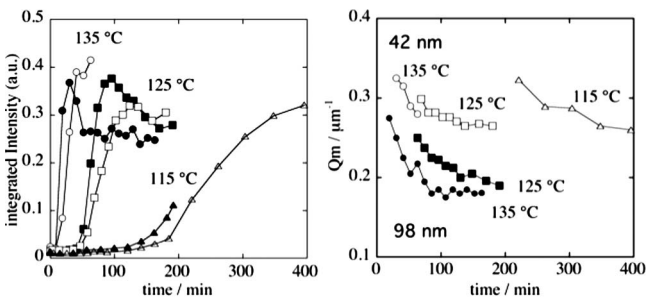


FIG. 11. Time evolution of (a) integrated peak intensity and (b) peak position for 98 and 42 nm blend thin films of dPS and PVME. (open circle): 42 nm, 135 °C, (closed circle): 98nm, 135 °C, (open square): 42 nm, 125 °C, (closed square): 98 nm, 125 °C, (open triangle): 42 nm, 115 °C, (closed triangle): 98 nm, 115 °C.

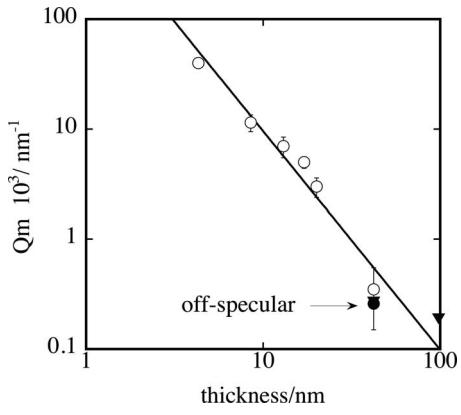


FIG. 13. Peak position $Q_m$ in FFT intensity profiles of AFM images for thin blend thin films of dPS and PVME after annealing at 115 °C for 30 min (open circle) as a function of initial film thickness. Peak positions of off-specular intensity $I(Q_x)$ at 115 °C (closed circle) and 125 °C (close triangle) are also shown.

## IV. CONCLUSION

In this work we have performed time-resolved specular and off-specular neutron reflectivity measurements on the dewetting process of dPS and PVME blend thin films in the two phase region using a TOF (or energy dispersive) neutron reflectometer. From the specular reflection we found that PVME thin layers were segregated to the air surface and the interface at Si substrate due to the preferential interactions even in the one phase region, and after the temperature jump into the two phase region phase separation of the middle blend layer proceeded in the depth direction ($z$ direction) during the incubation period before the dewetting. The phase separation in the depth direction did occur asymmetrically at the air and substrate sides and inhomogeneously in the film plane ($x$-$y$ direction), implying the dewetting in the present system occurs in the composition fluctuation mechanism. In the off-specular reflectivity measurements we observed structure formation process of droplets due to dewetting in micrometer scale in the film plane ($x$-$y$ direction). The present study shows that the TOF or energy dispersive reflectivity measurements give us very unique information on the structure formation in the film plane in addition to that in the depth direction.


[1] R. L. Jones and R. W. Richards, *Polymers at Surface and Interfaces* (Cambridge University Press, Cambridge, 1999).
[2] Polymer Surfaces, in *Interfaces and Thin Films*, edited by A. Karim and S. Kumar (World Scientific, Singapore, 2000).
[3] D. G. Bucknall, Prog. Mater. Sci. **49**, 713 (2004).
[4] P. Mueller-Buschbaum, E. Bauer, O. Wunnicke, and M. Stamm, J. Phys.: Condens. Matter **17**, S363 (2005).
[5] J. L. Keddie, R. A. Jones, and R. A. Cory, Europhys. Lett. **27**, 59 (1994).
[6] J. L. Keddie, R. A. Jones, and R. A. Cory, Faraday Discuss. **98**, 219 (1994).
[7] J. A. Forrest, K. Dalnoki-Veress, J. R. Stevens, and J. R. Dutcher, Phys. Rev. Lett. **77**, 2002 (1996).
[8] S. Kawana and R. A. L. Jones, Phys. Rev. E **63**, 021501 (2001).
[9] T. Miyazaki, K. Nishida, and T. Kanaya, Phys. Rev. E **69**, 061803 (2004).
[10] K. Dalnoki-Veress, J. A. Forrest, C. Murray, C. Giault, and J. R. Dutcher, Phys. Rev. E **63**, 031801 (2001).
[11] J. Mattsson, J. A. Forrest, and L. Borjesson, Phys. Rev. E **62**, 5187 (2000).
[12] P. Mueller-Buschbaum, S. A. O'Neill, S. Affrossman, and M. Stamm, Macromolecules **31**, 5003 (1998).
[13] H.-j. Chung and R. J. Composto, Phys. Rev. Lett. **92**, 185704 (2004).
[14] H. Wang and R. J. Composto, Europhys. Lett. **50**, 622 (2000).
[15] H. Wang and R. J. Composto, J. Chem. Phys. **113**, 10386 (2000).
[16] H. Wang and R. J. Composto, Interface Sci. **11**, 237 (2003).
[17] Y. Liao, Z. Su, Z. Sun, T. Shi, and L. An, Macromol. Rapid Commun. **27**, 351 (2006).
[18] K. Tanaka, J. S. Yoon, A. Takahara, and T. Kajiyama, Macromolecules **28**, 934 (1995).
[19] B. D. Ermi, A. Karim, and J. F. Douglas, J. Polym. Sci., Part. B: Polym. Phys. **36**, 191 (1998).
[20] A. Karim, T. M. Slawecki, S. K. Kumar, J. F. Douglas, S. K. Satija, C. C. Han, T. P. Russell, Y. Liu, R. Overnay, J. Sokolov, and M. H. Rafailovich, Macromolecules **31**, 857 (1998).
[21] K. El-Mabrouk, M. Belaiche, and M. Bousmina, J. Colloid Interface Sci. **306**, 354 (2007).
[22] H. Ogawa, T. Kanaya, K. Nishida, and G. Matsuba, Polymer **49**, 254 (2008).
[23] H. Ogawa, T. Kanaya, K. Nishida, and G. Matsuba, Polymer **49**, 2553 (2008).
[24] K. D. F. Wensink and B. Je'remoe, Langmuir **18**, 413 (2002).
[25] A. Sharma and J. Mittal, Phys. Rev. Lett. **89**, 186101 (2002).
[26] A. Sharma, J. Mittal, and R. Verma, Langmuir **18**, 10213 (2002).
[27] N. Clarke, Macromolecules **38**, 6775 (2005).
[28] H. j. Chung, K. Ohno, T. Fukuda, and T. J. Composto, Macromolecules **40**, 384 (2007).
[29] http://lansce.lanl.gov/lujan/instruments/spear/spear.htm
[30] Q. Bhatia, D. Pan, and J. Koberstein, Macromolecules **21**, 2166 (1988).
[31] J. Cowie, B. Devlin, and I. McEwen, Macromolecules **26**, 5628 (1993).
[32] S. Lee and C. Sung, Macromolecules **34**, 599 (2001).
[33] C. Forrey, J. Koberstein, and D. Pan, Interface Sci. **11**, 211 (2003).
[34] D. Kawaguchi, K. Tanaka, T. Kajiyama, A. Takahara, and S. Tasaki, Macromolecules **36**, 6824 (2003).
[35] R. A. L. Jones, L. J. Norton, E. J. Kramer, F. S. Bates, and P. Wiltzius, Phys. Rev. Lett. **66**, 1326 (1991).
[36] R. Inoue, T. Kanaya, K. Nishida, I. Tsukushi, and K. Shibata, Phys. Rev. Lett. **95**, 056102 (2005).
[37] R. Inoue, T. Kanaya, K. Nishida, I. Tsukushi, and K. Shibata, Phys. Rev. E **74**, 021801 (2006).
[38] K. Akabori, K. Tanaka, T. Nagamura, A. Takahara, and T. Kajiyama, Macromolecules **38**, 9735 (2005).
[39] T. Kanaya, R. Inoue, K. Kawashima, T. Miyazaki, I. Tsukushi, K. Shibata, G. Matsuba, K. Nishida, and M. Hino, J. Phys. Soc. Jpn. **78**, 041004 (2009).